The EMBO Journal Vol.18 No.11 pp.2941–2949, 1999

Functional glycan-free adhesion domain of human cell surface receptor CD58: design, production and NMR studies

Zhen-Yu J.Sun[1], Volker Dötsch[1,2], Mikyung Kim[3], Jing Li[3], Ellis L.Reinherz[3] and Gerhard Wagner[1,4]

[1]Department of Biological Chemistry and Molecular Pharmacology, Harvard Medical School and [3]Laboratory of Immunobiology, Dana-Farber Cancer Institute, Boston, MA 02115, USA

[2]Present address: Department of Pharmaceutical Chemistry, University of California at San Francisco, San Francisco, CA 94143, USA

[4]Corresponding author
e-mail: wagner@wagner.med.harvard.edu

A general strategy is presented here for producing glycan-free forms of glycoproteins without loss of function by employing apolar-to-polar mutations of surface residues in functionally irrelevant epitopes. The success of this structure-based approach was demonstrated through the expression in *Escherichia coli* of a soluble 11 kDa adhesion domain extracted from the heavily glycosylated 55 kDa human CD58 ectodomain. The solution structure was subsequently determined and binding to its counter-receptor CD2 studied by NMR. This mutant adhesion domain is functional as determined by several experimental methods, and the size of its binding site has been probed by chemical shift perturbations in NMR titration experiments. The new structural information supports a 'hand-shake' model of CD2–CD58 interaction involving the GFCC′C′′ faces of both CD2 and CD58 adhesion domains. The region responsible for binding specificity is most likely localized on the C, C′ and C′′ strands and the C–C′ and C′–C′′ loops on CD58.

Keywords: CD58/glycosylation/immunology/nuclear magnetic resonance/protein structure

Introduction

The human cell surface receptor CD58, also known as the lymphocyte function-associated antigen 3 (LFA-3), is the counter-receptor for the T-lymphocyte surface receptor CD2 (Seed, 1987; Selvaraj *et al*., 1987; Springer *et al*., 1987; Wallner *et al*., 1987). The initial binding of human CD58 to CD2 facilitates the adhesion between T lymphocytes and antigen-presenting cells (APC), and between cytolytic T cells, natural killer (NK) cells and their target cells (Siliciano *et al*., 1985; Dustin *et al*., 1987a; Plunkett *et al*., 1987; Moingeon *et al*., 1989). In addition, specific interactions between CD58 and CD2 play an important role via a CD2-mediated co-stimulatory pathway during T-cell activation and proliferation (Meuer *et al*., 1984; Koyasu *et al*., 1990; Schraven *et al*., 1990; Semnani *et al*., 1994; Teunissen *et al*., 1994; Wingren *et al*., 1995; Gollob *et al*., 1996). It has been shown that the CD2–CD58 interaction can reverse T-cell anergy (Boussiotis *et al*., 1994), and the blockade of CD2–CD58 interaction (Kaplon *et al*., 1996; Sultan *et al*., 1997) and/or modulation of the CD2 co-stimulatory pathway (Qin *et al*., 1994; Hirahara *et al*., 1995; Sido *et al*., 1996, 1997) can result in prolonged tolerance towards allografts. Thus, the structural studies of CD2–CD58 interaction have important implications for understanding protein–protein interaction and signal transduction as well as practical significance for establishing novel immunosuppressive modalities.

The 179-residue ectodomain of human CD58 consists of two extracellular immunoglobulin-like domains anchored to the membrane through either a transmembrane segment or a glycosyl phosphatidylinositol (GPI) linker (Dustin *et al*., 1987b; Wallich *et al*., 1998). The 95 residue membrane-distal N-terminal domain of CD58 (1dCD58) is entirely responsible for the adhesion to CD2. Although structural details of the human CD2 adhesion domain have been available through both NMR and X-ray crystallography studies (Withka *et al*., 1993; Bodian *et al*., 1994; Wyss *et al*., 1995), modeling of the CD2–CD58 interaction has been hindered by the lack of structural knowledge about the CD58 adhesion domain. The overall fold of the CD58 adhesion domain was predicted to be an immunoglobulin variable domain fold, and the ligand-binding site was mapped to the GFCC′C′′ face, similar to the adhesion domain of CD2 according to mutagenesis studies (Arulanandam *et al*., 1994; Osborn *et al*., 1995). However, the details about the amino acid residues involved in binding still await the experimental determination of the CD58 structure.

Human cell surface receptors, including CD58, are often modified by glycosylation that significantly increases structural complexity as well as overall molecular weight. The mature form of human CD58 is heavily glycosylated, with the carbohydrates accounting for 40–70% of the total molecular weight. The adhesion domain of CD58 alone contains three glycosylation sites, but the deglycosylated form has a mol. wt of 11.2 kDa, a size suitable for NMR spectroscopic studies. Deglycosylated proteins produced by endoglycosidase digestion can become unstable or inactive, and glycan-free proteins produced by bacterial expression are often insoluble and difficult to refold. Thus far, functional full-length and truncated CD58 constructs can only be expressed in mammalian cells. The problem of how to increase the stability and solubility of deglycosylated forms of glycoproteins in general is crucial for structural studies by NMR spectroscopy and X-ray crystallography. We report here the construction of a functional mutant adhesion domain of human CD58 using a structure-based rational mutagenesis strategy. This approach allows us to study the CD58 binding function using a soluble 11.2 kDa glycan-free adhesion domain

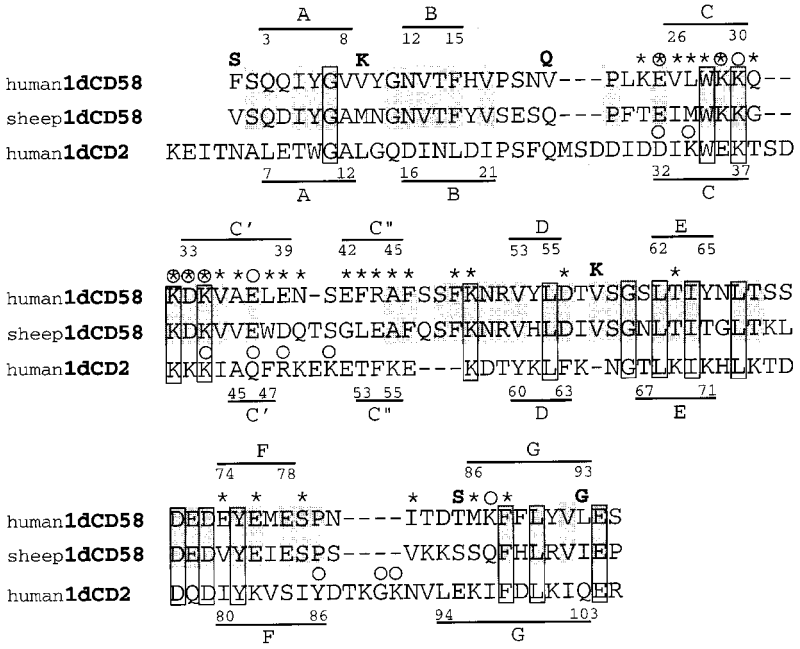

Fig. 1. Amino acid sequences for sheep 1dCD58, human 1dCD58 and 1dCD2. Conserved residues between sheep and human CD58 are shaded, while residues identical among all three sequences are boxed. The β-strands of human 1dCD58 and 1dCD2 are indicated based on NMR structural data. Mutant residues in human $1dCD58_{6m}$ are noted above the wild-type sequence. Residues implicated in human CD2–CD58 binding by mutagenesis studies are marked with circles (Peterson and Seed, 1987; Arulanandam *et al*., 1993b, 1994; Osborn *et al*., 1995). Residues of $1dCD58_{6m}$ shown to undergo significant chemical shift perturbation upon binding (index >0.5) are concentrated mostly on the C, C′ and C′′ strands and their connecting loops (marked by * symbols). For details, see text.

instead of a 55 kDa native glycosylated CD58 ectodomain. The high expression level of this glycan-free mutant in *Escherichia coli* enabled ^{15}N and ^{13}C isotopic labeling that greatly facilitated the structural determination and binding studies by NMR methods. Moreover, the strategy utilized here may be generally applicable for studies of many glycoproteins.

Results

Design and production of $1dCD58_{6m}$

The glycan-free wild-type 1dCD58 expressed from *E.coli* has a very low refolding efficiency and poor solubility. We reason that the absence of the carbohydrates leads to reduced protein solubility and aggregation, which could be compensated by apolar-to-polar substitutions of the surface-exposed hydrophobic residues. The adhesion domains of CD58 and CD2 both belong to the immunoglobulin variable domain superfamily and share 20% sequence homology at the amino acid level (Figure 1). Based on the solved structures of the adhesion domain of human CD2 (1dCD2) (Wyss *et al*., 1995), a molecular model of wild-type 1dCD58 has been constructed (Arulanandam *et al*., 1994). The results of alanine scanning (Arulanandam *et al*., 1994; Osborn *et al*., 1995) suggest that the CD2-binding epitope on CD58 can be mapped to the GFCC′C′′ face analogous to the CD58-binding site of CD2 (Arulanandam *et al*., 1993b; Somoza *et al*., 1993). Accordingly, five surface-exposed hydrophobic residues that are not involved in the binding function initially were identified from a total of 33 hydrophobic residues (excluding proline and glycine) in 1dCD58 (Figure 2A). Our strategy has been to replace these residues with charged and polar residues or glycine. Surface residues were also substituted by more hydrophilic ones that are present in the sheep CD58 sequence (Figure 1), as this homologous protein also binds to human CD2. The favorable substitutions inferred from sheep CD58 include Val21→Gln and Thr85→Ser (by eliminating a hydrophobic methyl group). The mutations of the remaining surface-exposed hydrophobic residues include: Phe1→Ser, Val9→Lys (with the possibility of forming a salt bridge with Glu94), Val58→Lys (forming a salt bridge with Asp56) and Leu93→Gly (with the additional benefit of more flexibility in the backbone to stabilize a potential salt bridge between Lys9 and Asp94). Altogether, the design of this soluble mutant adhesion domain of human CD58 contains six mutation sites (Figure 2B), all of which are predicted to lie outside the CD2-binding region.

This mutant adhesion domain of CD58 ($1dCD58_{6m}$) was expressed as inclusion bodies from *E.coli*, and purified subsequently after refolding. High pH and a high concentration of arginine in the refolding buffer are key to refolding efficiency. The final yield of the soluble $1dCD58_{6m}$ protein is 60 mg/l of cell culture, using a defined minimal medium containing NH_4Cl and glucose as the sole nitrogen and carbon source to facilitate isotopic labeling for NMR studies. Although the estimated pI value for $1dCD58_{6m}$ is as low as 5.1, the solubility of this mutant protein is relatively low at neutral pH (~3 mg/ml), but increases to 20 mg/ml (~1.8 mM) at pH 9.0. In addition, the protein is unfolded under acidic conditions. Since high pH causes increased amide proton exchange which complicates NMR experiments, as a compromise, the NMR samples were prepared at pH 7.5 in 10 mM $NaPO_4$, with protein concentrations at 7 mg/ml (0.6 mM).

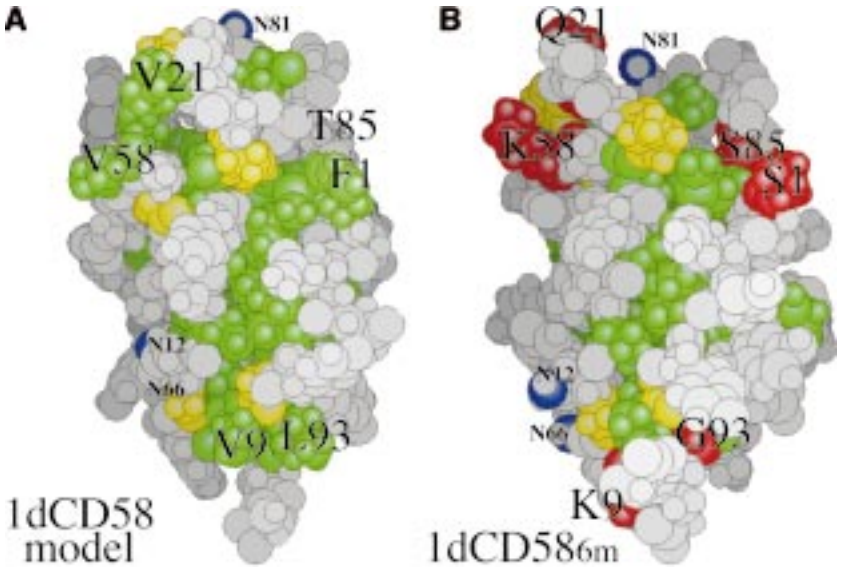

Fig. 2. Space-filling structural models for (**A**) a homology model of the wild-type adhesion domain of CD58 depicting surface-exposed hydrophobic residues and (**B**) the NMR structure of 1dCD58$_{6m}$ depicting mutation sites. The molecules are viewed edge-on, with β-strands A and B directly in the front. Proline and glycine residues are colored in yellow, other hydrophobic residues in green, mutation sites in red, and putative glycan attachment positions in blue. The graphs were prepared using GRASP (Nicholls *et al*., 1991).

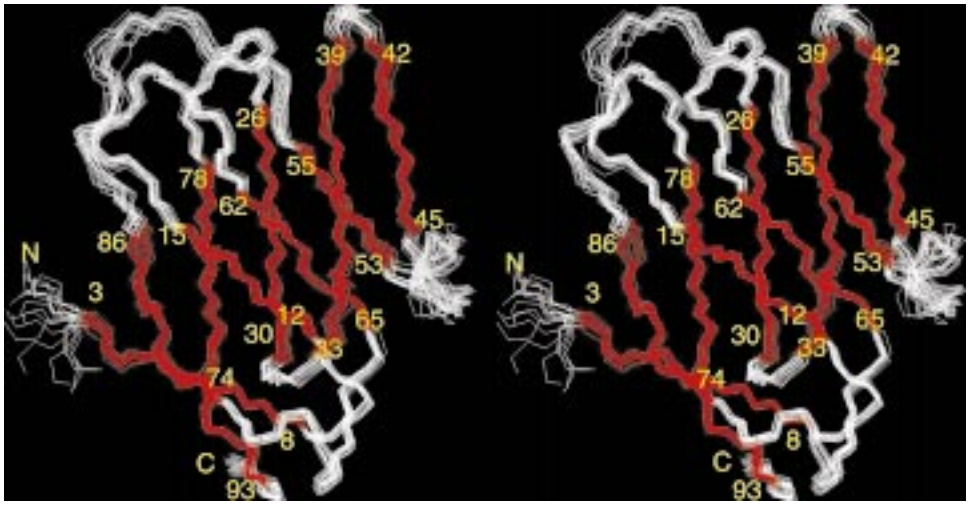

Fig. 3. Stereo diagram of backbone traces from 20 calculated structures of 1dCD58$_{6m}$ as viewed perpendicular to the β-sheets. The β-strands: A(3–8), B(12–15), C(26–30), C′(33–39), C′′(42–45), D(53–55), E(62–65), F(74–78) and G(86–93) are colored in red, with the first and last residues of each strand designated with yellow numbers. The N- and C-termini are also noted.

Solution structure determination by NMR

The solution structure of 1dCD58$_{6m}$ was solved by performing heteronuclear multi-dimensional NMR experiments with procedures described previously (Matsuo *et al*., 1997; Walters *et al*., 1997). The backbone traces of 20 calculated NMR structures of 1dCD58$_{6m}$ are shown in Figure 3. The adhesion domain of CD58 consists of nine β-strands forming two parallel β-sheets, in agreement with previous predictions (Arulanandam *et al*., 1994; Osborn *et al*., 1995). The β-sheet at the front where the ligand-binding site is located consists of strands A, G, F, C, C′ and C′′ with residues 3–8, 86–93, 74–78, 26–30, 33–39 and 42–45, respectively. The β-sheet at the back consists of strands B, E and D with residues 12–15, 62–65 and 53–55, respectively. All the strands in the β-sheets run antiparallel to each other except A and G. In addition, the C′′–D loop contains a short three-residue helical turn structure consisting of residues 49–51 (Figures 3 and 4A).

Several major structural differences exist between 1dCD58$_{6m}$ and 1dCD2 (Withka *et al*., 1993; Bodian *et al*., 1994; Wyss *et al*., 1995), although both adopt the same immunoglobulin variable domain fold (Figure 4A and C). First, the F–G loop in CD58 is shortened by four residues, and the β-bulge found in the G strand of CD2 is absent, creating a large depression on top of the G, F and C strands. Secondly, the lengths of the G, F and C strands are shorter than in CD2, while the C′ strand is extended to include a small β-bulge at Lys34. Thirdly, the C–C′ loop of CD58 is shortened by two residues, and the C′′ strand is more twisted towards the side. Taken together, the GFCC′C′′ face of CD58 containing the ligand-binding site is not as flat as that of CD2, but rather subdivided

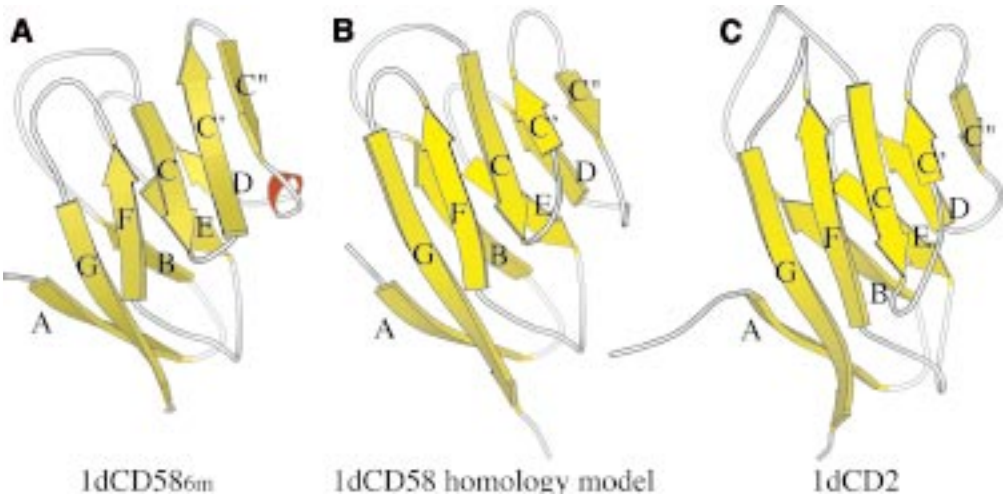

Fig. 4. Ribbon diagrams of (**A**) 1dCD58$_{6m}$, (**B**) homology model of wild-type 1dCD58 and (**C**) NMR structure of the wild-type adhesion domain of human CD2 (Withka *et al*., 1993; Bodian *et al*., 1994; Wyss *et al*., 1995). The graphs were prepared using MOLSCRIPT (Kraulis, 1991).

into two smaller GF and CC′C′′ faces joining to form a 150° angle. The differences in the lengths of the corresponding β-strands also suggest more flexibility in the FG area and more rigidity in the CC′C′′ area in CD58 compared with CD2. In addition, the C′′–D loop is three residues longer in CD58, and contains a short three-residue helical structure not present in CD2.

CD2 binding studies

A series of biochemical experiments confirmed that the glycan-free 1dCD58$_{6m}$ has the correct structural conformation and retains the adhesion function of the wild-type protein. First, 1dCD58$_{6m}$ was found to co-immunoprecipitate with TS2/9, a monoclonal antibody recognizing epitopes on the binding surface (FGCC′C′′ face) of the wild-type human CD58 (Dengler *et al*., 1992). Secondly, the binding of the two adhesion domains can be clearly shown by incubating 1dCD58$_{6m}$ with a hex-histidine-tagged human CD2 adhesion domain 1dCD2$_{r1}$ attached to Ni^{2+} beads. After washing away excess unbound 1dCD58$_{6m}$ and eluting with 0.5 M imidazole, two bands migrating at ~11 and 12.5 kDa molecular weights can be visualized on an SDS denaturing gel. Thirdly, the adhesion function of 1dCD58$_{6m}$ is demonstrated further in a rosetting experiment using the procedure described by Moingeon *et al*. (1989), where the clustering (rosetting) of sheep red blood cells (SRBC) (expressing sheep CD58) around T-cell hybridomas expressing human CD2 can be blocked by the addition of 1dCD58$_{6m}$. This binding assay indicates that 50% inhibition of the cell rosetting can be achieved at a 1dCD58$_{6m}$ concentration of 0.25 μM, a binding strength comparable with that of the wild-type interaction (0.4 μM) (Sayre *et al*., 1989). In addition, preliminary results from an isothermal titration calorimetry study of interaction between 1dCD58$_{6m}$ and 1dCD2$_{r1}$ indicate an equilibrium dissociation constant K_D of the order of 0.2 μM (unpublished data), consistent with the results from the rosetting experiment.

The submicromolar binding affinity of the glycan-free 1dCD58$_{6m}$ with CD2 enabled us to perform NMR binding experiments to study structural features of the CD2–CD58 interaction. The ^{15}N–^{1}H heteronuclear single quantum correlation (HSQC) spectra of three samples were recorded at 25°C for uniformly ^{15}N-labeled 1dCD58$_{6m}$ in the uncomplexed form, 50% complexed, i.e. by mixing [^{15}N]1dCD58$_{6m}$ with the unlabeled adhesion domain of CD2 (1dCD2$_{r2}$) at a 2:1 molar ratio, and 100% complexed with excess unlabeled 1dCD2$_{r2}$ (Figure 5A). New resonance peaks from the backbone amide groups of [^{15}N]1dCD58$_{6m}$ complexed with 1dCD2$_{r2}$ emerge, and peak intensities from the uncomplexed 1dCD58$_{6m}$ decrease as a function of increasing 1dCD2$_{r2}$ concentration (e.g. resonances from Asp33 and Ala45 in Figure 5A). The appearance of doublets from both complexed and uncomplexed [^{15}N]1dCD58$_{6m}$ in the 50% complexed sample indicates slow NMR exchange kinetics (e.g. resonance from Asp84 in Figure 5A, middle section). The dissociation rate (k_{off}) of the 1dCD2$_{r2}$–1dCD58$_{6m}$ complex is estimated to be 7/s as derived from an exchange line broadening of 2.1 ± 0.4 Hz. This direct measurement of k_{off} is in agreement with the value (>5/s) estimated from using surface plasmon resonance (van der Merwe *et al*., 1994). It is interesting that a similar NMR study suggests a much faster dissociation rate for the complex of the adhesion domains of rat CD2 and CD48 (McAlister *et al*., 1996), which is consistent with the fact that the binding strength of the human CD2–CD58 interaction is >10-fold greater than that of the rat CD2–CD48 interaction (van der Merwe *et al*., 1993; Davis *et al*., 1998), and at least two orders of magnitude greater than that of the human CD2–CD48 interaction (Arulanandam *et al*., 1993a).

Discussion

In this study, we show that the need for glycosylation of a functional CD58 adhesion domain can be eliminated entirely by hydrophobic-to-hydrophilic mutations of a small subset of surface residues in regions that are not relevant for receptor recognition. Our homology modeled structure of 1dCD58 for selecting mutation sites (Arulanandam *et al*., 1994) agrees reasonably well with the experimentally determined NMR structure of 1dCD58$_{6m}$ (Figure 4A and B), with an average backbone root-mean-square deviation (r.m.s.d.) of 1.7 Å from the mean NMR

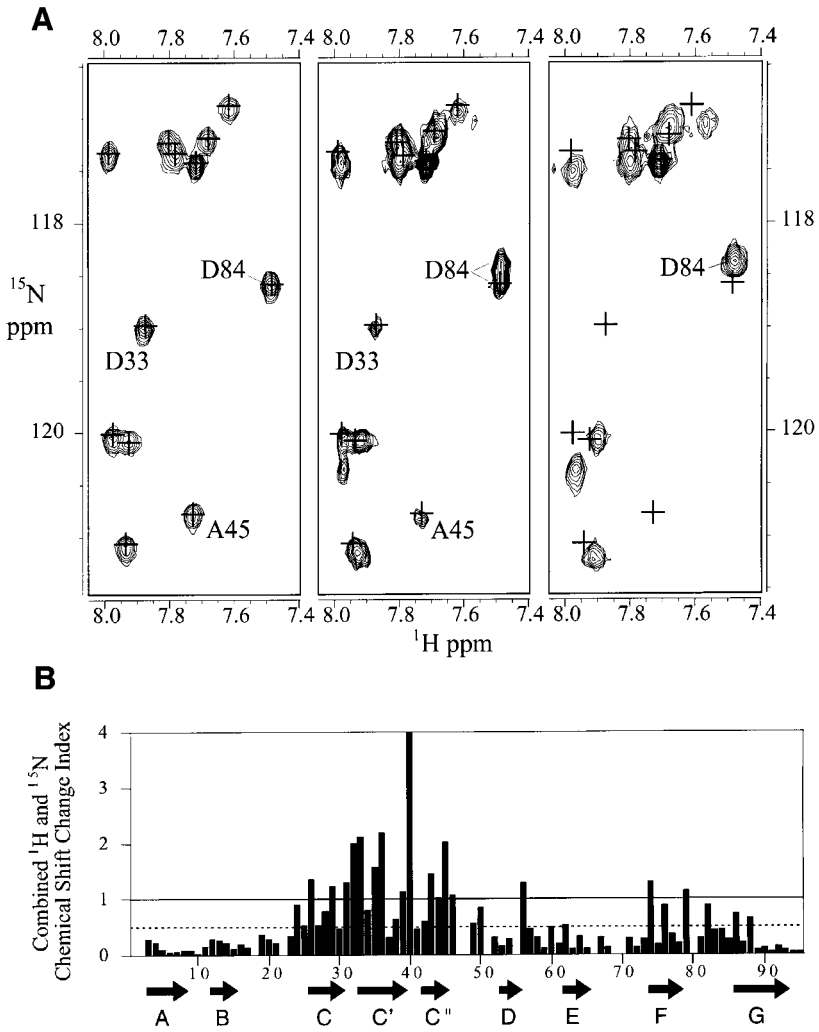

Fig. 5. NMR chemical shift data of 1dCD58$_{6m}$ upon binding to CD2. (**A**) Selected regions from the ^{1}H–^{15}N HSQC spectra of 0.5 mM uncomplexed ^{15}N-labeled 1dCD58$_{6m}$ (left), 0.2 mM ^{15}N-labeled 1dCD58$_{6m}$ (50% complexed) with 0.1 mM unlabeled 1dCD2$_{r2}$ (middle) and 0.2 mM ^{15}N-labeled 1dCD58$_{6m}$ (100% complexed) with 0.22 mM unlabeled 1dCD2$_{r2}$ (right). The '+' signs indicate the resonance peak positions from uncomplexed 1dCD58$_{6m}$. All spectra were recorded using a Bruker AMX-500 spectrometer at 25°C. (**B**) The lower limit estimates of chemical shift perturbation of ^{15}N-labeled 1dCD58$_{6m}$ upon binding to CD2 (see text for details) plotted against the amino acid sequence. The combined index of chemical shift change is determined by: $[(\Delta^{1}\text{H\_cs})^2 + (\Delta^{15}\text{N\_cs})^2]^{1/2}$, where Δ^{1}H_cs of proton resonance is in units of 0.1 p.p.m., and Δ^{15}N_cs of nitrogen resonance is in units of 0.5 p.p.m. A solid line indicates an index of 1.0, and a dashed line an index of 0.5.

structure. The surface exposure and environment of the six mutation sites in 1dCD58$_{6m}$ are similar to those predicted from the homology model (Figure 2). Overall, our strategy of replacing the surface-exposed hydrophobic residues with more hydrophilic ones was successful in increasing the solubility of a glycan-free 1dCD58. Although similar approaches have been reported previously to increase the solubility of single chain T-cell receptor and antibody 4-4-20 fragments (Novotny *et al*., 1991; Nieba *et al*., 1997), to the best of our knowledge, this is the first application towards compensating the effects of the removal of carbohydrates in glycoproteins. The design of this functional CD58 adhesion domain was achieved through a single step. The contribution of individual mutations awaits to be assessed in future experiments, and additional mutations of other partially exposed hydrophobic residues may be employed to increase the protein solubility further.

Detailed structural information about protein-binding sites can be obtained from NMR binding studies (Otting, 1993; Fejzo *et al*., 1994; Osborne *et al*., 1997 and references therein). Although the new resonances from the complexed [^{15}N]1dCD58$_{6m}$ cannot be traced continuously from the assigned backbone amide peaks from the uncomplexed [^{15}N]1dCD58$_{6m}$ due to the slow NMR exchange kinetics, we can still gauge the size of the CD2-binding region of 1dCD58$_{6m}$ from the estimated lower limits of chemical shift perturbation of each residue (i.e. by measuring the chemical shift differences between the assigned peaks from the uncomplexed [^{15}N]1dCD58$_{6m}$ and its closest adjacent peak from the complexed [^{15}N]1dCD58$_{6m}$). The regions in 1dCD58$_{6m}$ that show the most significant chemical shift perturbation include the C, C′ and C′′ strands, and the C–C′ and C′–C′′ loops (Figure 5B). Six residues on the F and G strands and the F–G loop also show chemical shift perturbations to a lesser extent. Among them, the amide protons of Glu74 and Glu76 are hydrogen bonded to the C strand, while Ser79, Ile82, Met86 and Phe88 all have buried side chains, suggesting indirect binding effects. Residues with strong

(index >1.0) and medium (index >0.5) chemical shift perturbations upon binding are compared with previous mutagenesis data of wild-type CD58 (Arulanandam *et al*., 1994) (Figure 6A and B). The common set of residues implicated from both results include Glu25, Lys29, Lys32, Asp33 and Lys34 on the C and C′ strands and the C–C′ loop. In contrast, previous mutagenesis data suggest that the residues determining CD58-binding specificity on CD2 are probably located on the upper half of the GFCC′C′′ face (Figure 6D). However, the comparison of amino sequences of human and sheep CD58 (both bind to human CD2) suggests that while the residues in the C and C′ strands and the C–C′ loop are mostly conserved, the C′–C′′ and F–G loops on the upper half of the GFCC′C′′ face are among the least conserved regions (Figure 1). The specific roles of the charged residues in these regions are discussed below.

It is well known that the charged residues on the GFCC′C′′ faces of both human 1dCD2 and 1dCD58 play an important role in their binding function (Arulanandam *et al*., 1993b, 1994; Somoza *et al*., 1993; Osborn *et al*., 1995; Davis *et al*., 1998). The electrostatic potential surface maps of 1dCD58$_{6m}$ and wild-type 1dCD2 show that the upper half of the binding face on CD58 is particularly negatively charged, complementing the right half of the binding face on CD2, which is positively charged (Figure 6C and D). A homology model of sheep 1dCD58 (with 50% sequence homology) based on the solved NMR structure of human 1dCD58$_{6m}$ shows that the electrostatic potential maps of both binding surfaces are nearly identical. Six of the nine negatively charged residues on the GFCC′C′′ face of human 1dCD58 are conserved or preserved as negatively charged residues in sheep 1dCD58. Five of these residues, Glu25, Glu37, Glu39, Glu76 and Glu78, are clustered around a concave region that is absent in the CD2 structure due to the presence of a β-bulge on the G strand; but only Glu37 shows a strong effect of disrupting CD2 binding by alanine scanning (Arulanandam *et al*., 1994) (Figure 6B and C). Thus, in contrast to the residues around the C–C′ loop that are more crucial for ligand recognition (Figure 6B), the negatively charged residues in or around this concave region on CD58 may have additional roles. First, concentrated same-charge residues could enhance long-range electrostatic interactions to guide the docking of the two counter receptors. Furthermore, the clustering of hydrophilic residues with the same type of charge induces unfavorable electrostatic repulsion and also significantly

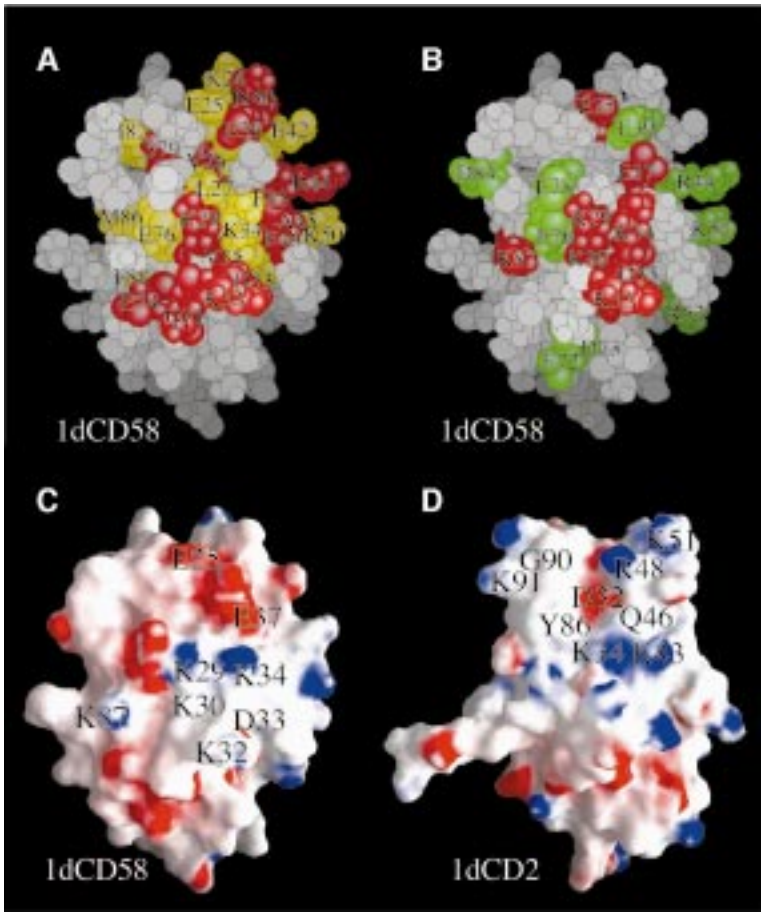

Fig. 6. Mapping of the CD2-binding site on CD58. The panel at the top shows the ligand-binding face of 1dCD58$_{6m}$ with (**A**) residues that show strong (index >1.0, in red) and medium (index >0.5, in yellow) chemical shift perturbation upon binding to CD2, and (**B**) residues that are implicated in CD2 binding (in red) or without effect (in green) based upon alanine scanning mutagenesis, as derived from Arulanandam *et al*. (1994). The panel at the bottom shows the surface maps of electrostatic potential on the ligand-binding faces of (**C**) 1dCD58$_{6m}$ and (**D**) wild-type 1dCD2 (Withka *et al*., 1993; Bodian *et al*., 1994; Wyss *et al*., 1995). Negatively charged regions are colored in red, positively charged regions in blue. Residues implicated in binding by previous mutagenesis studies are marked to illustrate the putative binding sites, as derived from Peterson and Seed (1987), Arulanandam *et al*. (1993b, 1994) and Osborn *et al*. (1995). The graphs were prepared using GRASP (Nicholls *et al*., 1991).

reduces the degree of solvation compared with a fully exposed and well-dispersed arrangement. Thus, these negatively charged residues concentrated in or around this concave region on CD58 may contribute a substantial amount of binding energy by replacing the surrounding solvent water molecules with more favorable electrostatic interactions when buried in the interface of a CD2–CD58 complex.

Our findings support a 'hand-shake' binding model, in which the CD2 and CD58 adhesion domains approach each other from opposite ends in an orthogonal orientation, similar to the dimer contact found in the human and rat CD2 crystal structures (Jones *et al*., 1992; Bodian *et al*., 1994). In this binding mode, the right half of their GFCC′C′′ binding face (C, C′ and the C–C′ loop) is roughly contacting the upper half (F–G loop region) of its partner. The lack of a large hydrophobic surface and the strong electrostatic interaction at the protein-binding sites appear to be the principal factors determining the CD2–CD58 binding affinity and kinetics. The 0.25 μM binding constant and 7/s dissociation rate suggest a fast association rate. These characteristics are remarkably well suited for CD2 and CD58 receptors to initiate and maintain dynamic contacts between T lymphocytes and NK cells and their targets. For comparison, the affinity between human CD2 and human CD48, a second ligand for CD2, is extremely low and unable to support cell-based adhesion (Arulanandam *et al*., 1993a). On the other hand, a CD58 gene has not yet been found in mouse and rat, and the only counter-receptor for CD2 identified so far is CD48. It is therefore likely that CD58 has evolved in a later stage of evolution as a result of gene duplication from CD48 to become a dedicated counter-receptor for CD2 (Wong *et al*., 1990; Arulanandam *et al*., 1993a). The study of different complexes of CD2 with their ligands can be used for modeling protein interaction by detailing the contribution of individual residues at the binding site in terms of binding specificity and/or kinetics. The unique involvement of a large percentage of charged residues in CD2–CD58 binding could be exploited to study the effect of electrostatic interactions on binding affinity by mutants designed from protein engineering.

In summary, we have shown that the requirement for glycosylation for the adhesion function of human CD58 can be eliminated by judicious hydrophobic-to-hydrophilic mutations of surface residues that are non-essential for recognition function. Introduction of six mutations in a single design step made possible expression in *E.coli* of a functional and highly soluble CD58 adhesion domain, for which a solution structure could be determined. The glycan-free $1dCD58_{6m}$ forms a tight and highly soluble complex with 1dCD2 showing slow NMR exchange kinetics. Comparison of surface properties of $1dCD58_{6m}$ and the adhesion domain of human CD2, together with results from NMR binding experiments, reveal a shape and charge complementarity, and support a 'hand-shake' model for the CD2–CD58 interaction that relies mainly on electrostatic interactions. The approach of substituting the solubilization function of glycans with hydrophobic-to-hydrophilic mutations may be generally applicable to produce and study other functional deglycosylated forms of glycoproteins that suffer from solubility problems.

Materials and methods

The DNA encoding the mutant $1dCD58_{6m}$ protein was synthesized by PCR to link eight overlapping oligonucleotides. The gene was then cloned into the pET11a vector (Novagen, Madison, WI) and expressed in *E.coli* BL21(DE3) strain. The mutant $1dCD58_{6m}$ was produced as inclusion bodies after induction by 1 mM isopropyl-β-D-thiogalactopyranoside (IPTG) at 37°C. The inclusion bodies isolated from the cell lysate were dissolved in 6 M guanidine HCl, and refolded by a simple two-step dilution procedure using 0.8 M arginine, 20 mM EDTA, 0.2 M Tris buffer, pH 9.5. Large misfolded aggregates were removed by passing purified protein through a Superdex-75 gel filtration column (Pharmacia, Piscataway, NJ). Two variant adhesion domains of human CD2 were constructed both containing three mutations, Lys61→Glu, Phe63→Leu and Thr67→Ala, to compensate for stability in the absence of glycans (Wyss *et al*., 1995), and will be reported elsewhere. The mutant $1dCD2_{r1}$ contains a hex-histidine tag at the C-terminus, while $1dCD2_{r2}$ used in the NMR binding studies contains two extra residues Gly and Ser at the N-terminus from thrombin cleavage. These two glycan-free mutant CD2 adhesion domains expressed from *E.coli* are both stable and functional.

TS2/9 monoclonal antibody used in the immunoprecipitation experiment is a kind gift of Dr T.A.Springer (Center for Blood Research and Harvard Medical School, Boston, MA). The cell rosetting experiment was performed using the procedure described previously (Moingeon *et al*., 1989). The SRBC, purchased from BioWhittacker Inc. (Walkersville, MD), were pre-incubated for 15 min at 37°C with aminoethylisothiouronium bromide (AET) (Sigma, St Louis, MO), washed four times and resuspended 1:20 in RPMI buffer + 2% fetal calf serum (FCS) (Life Technologies, Grand Island, NY). After adding 10 μl of pre-treated SRBC to 10^5 cells of a human CD2-expressing T-cell hybridoma to a final volume of 80 μl, the cells were incubated at 30°C for 5 min, spun down and incubated again at 4°C for 1 h. After gentle resuspension, they were placed on glass slides, and ~200 cells were observed under the microscope; those cells with at least five SRBC bound were counted as rosette-positive.

NMR data for resonance assignments were obtained at 25°C using Bruker and Varian spectrometers with a ^1H operating frequency of 500 MHz. The protein backbone amide assignments were obtained from ^{15}N-NOESY-HSQC experiments, and heteronuclear 3D HNCA (Kay *et al*., 1990) and CBCA(CO)NH (Grzesiek and Bax, 1992) experiments using a uniformly ^{15}N,^{13}C-double-labeled sample. Initial assignments were facilitated by HSQC experiments of samples selectively labeled with [^{15}N]Leu, [^{15}N]Val, [^{15}N]Ile, [^{15}N]Phe or [^{15}N]Tyr using a *E.coli*

Table I. Structural statistics for 20 NMR structures[a]

NOE distance restraints	
Intraresidue	290
Medium range [(*i*–*j*) ≤4]	418
Long range [(*i*–*j*) >4]	570
Total	1278
Hydrogen bonds	30
Dihedral angle restraints	99
Ramachandran plot[b]	
(residues 3–95)	
Most favored region	71.6%
Additionally allowed region	24.9%
Generously allowed region	3.1%
Disallowed region[c]	0.4%
R.m.s.d. from ideal geometry	
Bonds (Å)	0.001 ± 0.00004
Angles (°)	0.31 ± 0.002
Impropers (°)	0.15 ± 0.005
R.m.s.d. from mean structure	
(residues 3–95)	
Backbone (Å)	0.37 ± 0.05
Heavy atoms (Å)	0.93 ± 0.07

[a]The 20 structures with lowest energy selected from 25 calculated final structures by X-PLOR (Brünger, 1992) contain no distance violations greater than 0.3 Å, and no dihedral angle violations >5°.
[b]Data obtained by using the program PROCHECK-NMR (Laskowski *et al*., 1996).
[c]The residues (Asn20, Gln21 and Ser47) that appear in the disallowed regions are located in the flexible loop regions where few NMR restraints are observed.

DL39 strain. Side chain assignments were obtained from HBHA(CBCA-CO)NH (Grzesiek and Bax, 1993), CBCA(CO)NH and HCCH-TOCSY experiments (Kay *et al*., 1993). Distance constraints were obtained from a 2D NOESY in D_2O and a 3D ^{15}N-NOESY-HSQC experiment in H_2O with 60 ms mixing time using a Varian Unity-Inova 750 MHz spectrometer. Additional data were obtained from HNHA (Vuister and Bax, 1993) and HNHB (Archer *et al*., 1991) experiments for torsion angle constraints, and ^{13}C-HSQC experiment using a 10% ^{13}C-labeled sample for stereospecific assignments of all the methyl groups (Neri *et al*., 1989).

NMR data processing and analysis were carried out using the PROSA (Güntert *et al*., 1992), XEASY (Bartels *et al*., 1995) and DIANA software packages (Güntert and Wüthrich, 1991). Structural calculation by simulated annealing was performed by using DYANA (Güntert *et al*., 1997) and X-PLOR software (Brünger, 1992) using 1278 NOE distance, 30 hydrogen bond and 99 dihedral angle constraints (converted by DIANA). Results of structural refinement from 20 final annealed structures (Figure 3) with the lowest energy calculated by X-PLOR are listed in Table I. The secondary structures were confirmed primarily by using the PROCHECK-NMR software (Laskowski *et al*., 1996), and also taking into account the ^{1}H and ^{13}C chemical shift indexes (Wishart and Sykes, 1994).

The NMR spectra of ^{15}N-labeled 1dCD58$_{6m}$ in complex with 1dCD2$_{r2}$ were obtained on a 500 MHz Bruker spectrometer. The exchange rate between the complexed and uncomplexed 1dCD58$_{6m}$ is slow on an NMR time scale. The resulting additional exchange line broadening ($\delta\Delta\nu$) is related to the exchange rate k_{ex} by: $k_{ex} = \pi \cdot \delta\Delta\nu$ (Cavanagh *et al*., 1996), provided that the separation of the two peaks in exchange is much greater than $\delta\Delta\nu$. Out of 38 resonance peaks of the complexed 1dCD58$_{6m}$ that are well resolved from the uncomplexed 1dCD58$_{6m}$ (roughly corresponding to a combined chemical shift change index >0.5; see Figure 5B), nine have been assigned unambiguously. The average value of $\delta\Delta\nu$ was estimated by measuring 14 line-width differences (in the resolved ^{1}H and ^{15}N dimensions) of the corresponding nine assigned peaks from the uncomplexed 1dCD58$_{6m}$ in the 50% complexed sample and the 1dCD58$_{6m}$ alone sample. The dissociation rate k_{off} of the CD2–CD58 complex is equal to k_{ex} in this 50% complexed sample.

Acknowledgements

We thank G.Heffron for technical assistance, and C.Freund and J.D.Gross for helpful suggestions and critical comments. The coordinates of 1dCD58$_{6m}$ have been deposited in the Protein Data Bank (PDB ID 1ci5). This work was supported by National Institute of Health (NIH) NRSA fellowship to Z.-Y.J.S. Support from NIH grants AI37581 to G.W. and AI21226 to E.L.R. is gratefully acknowledged. Acquisition and maintenance of spectrometers and computers used for this work were supported by the National Science Foundation (MCB 9527181), the Harvard Center for Structural Biology and the Giovanni Armenise–Harvard Foundation for Advanced Scientific Research.

References

Archer,S.J., Ikura,M., Torchia,D.A. and Bax,A. (1991) An alternative 3D NMR technique for correlating backbone ^{15}N with side chain Hβ resonances in larger proteins. *J. Magn. Resonance*, **95**, 636–641.

Arulanandam,A.R.N., Moingeon,P., Concino,M.F., Recny,M.A., Kato,K., Yagita,H., Koyasu,S. and Reinherz,E.L. (1993a) A soluble multimeric recombinant CD2 protein identifies CD48 as a low affinity receptor for human CD2: divergence of CD2 ligands during the evolution of humans and mice. *J. Exp. Med.*, **177**, 1439–1450.

Arulanandam,A.R.N., Withka,J.M., Wyss,D.F., Wagner,G., Kister,A., Pallai,P., Recny,M.A. and Reinherz,E.L. (1993b) The CD58 (LFA-3) binding site is a localized and highly charged surface area on the AGFCC′C′′ face of the human CD2 adhesion domain. *Proc. Natl Acad. Sci. USA*, **90**, 11613–11617.

Arulanandam,A.R.N., Kister,A., McGregor,M.J., Wyss,D.F., Wagner,G. and Reinherz,E.L. (1994) Interaction between human CD2 and CD58 involves the major β sheet surface of each of their respective adhesion domains. *J. Exp. Med.*, **180**, 1861–1871.

Bartels,C., Xia,T., Billeter,M., Güntert,P. and Wüthrich,K. (1995) The program XEASY for computer-supported NMR spectral analysis of biological macromolecules. *J. Biomol. NMR*, **6**, 1–10.

Bodian,D.L., Jones,E.Y., Harlos,K., Stuart,D.I. and Davis,S.J. (1994) Crystal structure of the extracellular region of the human cell adhesion molecule CD2 at 2.5 Å resolution. *Structure*, **2**, 755–766.

Boussiotis,V.A., Freeman,G.J., Griffin,J.D., Gray,G.S., Gribben,J.G. and Nadler,L.M. (1994) CD2 is involved in maintenance and reversal of human alloantigen-specific clonal anergy. *J. Exp. Med.*, **180**, 1665–1673.

Brünger,A.T. (1992) *X-PLOR Version 3.1: A System for X-ray Crystallography and NMR*. Yale University Press, New Haven, CT.

Cavanagh,J., Fairbrother,W.J., Palmer,A.G. and Skelton,N.J. (1996) *Protein NMR Spectroscopy.* Academic Press, San Diego, CA.

Davis,S.J., Ikemizu,S., Wild,M.K. and van der Merwe,P.A. (1998) CD2 and the nature of protein interactions mediating cell–cell recognition. *Immunol. Rev.*, **163**, 217–236.

Dengler,T.J., Hoffmann,J.C., Knolle,P., Albert-Wolf,M., Roux,M., Wallich,R. and Meuer,S.C. (1992) Structural and functional epitopes of the human adhesion receptor CD58 (LFA-3). *Eur. J. Immunol.*, **22**, 2809–2817.

Dustin,M.L., Sanders,M.E., Shaw,S. and Springer,T.A. (1987a) Purified lymphocyte function-associated antigen 3 binds to CD2 and mediates T lymphocyte adhesion. *J. Exp. Med.*, **165**, 677–692.

Dustin,M.L., Selvaraj,P., Mattaliano,R.J. and Springer,T.A. (1987b) Anchoring mechanisms for LFA-3 cell adhesion glycoprotein at membrane surface. *Nature*, **329**, 846–848.

Fejzo,J., Etzkorn,F.A., Clubb,R.T., Shi,Y., Walsh,C.T. and Wagner,G. (1994) The mutant *Escherichia coli* F112W cyclophilin binds cyclosporin A in nearly identical conformation as human cyclophilin. *Biochemistry*, **33**, 5711–5720.

Gollob,J.A., Li,J., Kawasaki,H., Daley,J.F., Groves,C., Reinherz,E.L. and Ritz,J. (1996) Molecular interaction between CD58 and CD2 counter-receptors mediates the ability of monocytes to augment T cell activation by IL-12. *J. Immunol.*, **157**, 1886–1893.

Grzesiek,S. and Bax,A. (1992) Correlating backbone amide and side chain resonances in larger proteins by multiple relayed triple resonance NMR. *J. Am. Chem. Soc.*, **114**, 6291–6293.

Grzesiek,S. and Bax,A. (1993) Amino acid type determination in the sequential assignment procedure of uniformly ^{13}C/^{15}N-enriched proteins. *J. Biomol. NMR*, **3**, 185–204.

Güntert,P. and Wüthrich,K. (1991) Improved efficiency of protein structure calculations from NMR data using the program DIANA with redundant dihedral angle constraints. *J. Biomol. NMR*, **1**, 447–456.

Güntert,P., Dötsch,V., Wider,G. and Wüthrich,K. (1992) Processing of multi-dimensional NMR data with the new software PROSA. *J. Biomol. NMR*, **2**, 619–629.

Güntert,P., Mumenthaler,C. and Wüthrich,K. (1997) Torsion angle dynamics for NMR structure calculation with the new program DYANA. *J. Mol. Biol.*, **273**, 283–298.

Hirahara,H., Tsuchida,M., Wanatabe,T., Haga,M., Matsumoto,Y., Abo,T. and Eguchi,S. (1995) Long-term survival of cardiac allografts in rats treated before and after surgery with monoclonal antibody to CD2. *Transplantation*, **59**, 85–90.

Jones,E.Y., Davis,S.J., Williams,A.F., Harlos,K. and Stuart,D.I. (1992) Crystal structure at 2.8 Å resolution of a soluble form of the cell adhesion molecule CD2. *Nature*, **360**, 232–239.

Kaplon,R.J. *et al*. (1996) Short course single agent therapy with an LFA-3–IgG1 fusion protein prolongs primate cardiac allograft survival. *Transplantation*, **61**, 356–363.

Kay,L.E., Ikura,M., Tschudin,R. and Bax,A. (1990) Three-dimensional triple-resonance NMR spectroscopy of isotopically enriched proteins. *J. Magn. Resonance*, **89**, 496–514.

Kay,L.E., Xu,G., Singer,A.U., Muhandiram,D.R. and Forman-Kay,J.D. (1993) A gradient-enhanced HCCH-TOCSY experiment for recording side-chain ^{1}H and ^{13}C correlations in H_2O samples of proteins. *J. Magn. Resonance*, **B101**, 333–337.

Koyasu,S., Lawton,T., Novick,D., Recny,M.A., Siliciano,R.F., Wallner,B.P. and Reinherz,E.L. (1990) Role of interaction of CD2 molecule with lymphocyte function-associated antigen 3 in T-cell recognition of nominal antigen. *Proc. Natl Acad. Sci. USA*, **87**, 2603–2607.

Kraulis,P.J. (1991) MOLSCRIPT: a program to produce both detailed and schematic plots of protein structures. *J. Appl. Crystallogr.*, **24**, 946–950.

Laskowski,R.A., Rullmann,J.A.C., MacArthur,M.W., Kaptein,R. and Thornton,J.M. (1996) AQUA and PROCHECK-NMR: programs for checking the quality of protein structures solved by NMR. *J. Biomol. NMR*, **8**, 477–486.

Matsuo,H., Li,H., McGuire,A.M., Fletcher,C.M., Gingras,A.-C., Sonenberg,N. and Wagner,G. (1997) Structure of translation factor eIF4E bound to m7GDP and interaction with 4E-binding protein. *Nature Struct. Biol.*, **4**, 717–724.

McAlister,M.S.B., Mott,H.R., van der Merwe,P.A., Campbell,I.D., Davis,S.J. and Driscoll,P.C. (1996) NMR analysis of interacting soluble forms of the cell–cell recognition molecules CD2 and CD48. *Biochemistry*, **35**, 5982–5991.

Meuer,S.C. *et al*. (1984) An alternative pathway of T cell activation: a functional role for the 50 kD T11 sheep erythrocyte receptor protein. *Cell*, **36**, 897–906.

Moingeon,P., Chang,H.-C., Wallner,B.P., Stebbins,C., Frey,A.Z. and Reinherz,E.L. (1989) CD2-mediated adhesion facilitates T lymphocyte antigen recognition function. *Nature*, **339**, 312–314.

Neri,D., Szyperski,T., Otting,G., Senn,H. and Wüthrich,K. (1989) Stereospecific nuclear magnetic resonance assignments of the methyl groups of valine and leucine in the DNA-binding domain of the 434 repressor by biosynthetically directed fractional ^{13}C labeling. *Biochemistry*, **28**, 7510–7516.

Nicholls,A., Sharp,K. and Honig,B. (1991) Protein folding and association: insights from the interfacial and thermodynamic properties of hydrocarbons. *Proteins Struct. Funct. Genet.*, **11**, 282–293.

Nieba,L., Honegger,A., Krebber,C. and Plückthun,A. (1997) Disrupting the hydrophobic patches at the antibody variable/constant domain interface: improved *in vivo* folding and physical characterization of an engineered scFv fragment. *Protein Eng.*, **10**, 435–444.

Novotny,J., Ganju,R.K., Smiley,S.T., Hussey,R.E., Luther,M.A., Recny,M.A., Siliciano,R.F. and Reinherz,E. (1991) A soluble, single-chain T-cell receptor fragment endowed with antigen-combining properties. *Proc. Natl Acad. Sci. USA*, **88**, 8646–8650.

Osborn,L., Day,E.S., Miller,G.T., Karpusas,M., Tizard,R., Meuer,S.C. and Hochman,P.S. (1995) Amino acid residues required for binding of lymphocyte function-associated antigen 3 (CD58) to its counter-receptor CD2. *J. Exp. Med.*, **181**, 429–434.

Osborne,M.J., Wallis,R., Leung,K.-Y., Williams,G., Lian,L.-Y., James,R., Kleanthous,C. and Moore,G.R. (1997) Identification of critical residues in the colicin E9 DNase binding region of the Im9 protein. *Biochem. J.*, **323**, 823–831.

Otting,G. (1993) Experimental NMR techniques for studies of protein–ligand interactions. *Curr. Opin. Struct. Biol.*, **3**, 760–768.

Peterson,A. and Seed,B. (1987) Monoclonal antibody and ligand binding sites of the T cell erythrocyte receptor (CD2). *Nature*, **329**, 842–846.

Plunkett,M.L., Sanders,M.E., Selvaraj,P., Dustin,M.L. and Springer,T.A. (1987) Rosetting of activated human T lymphocytes with autologous erythrocytes. Definition of the receptor and ligand molecules as CD2 and lymphocyte function-associated antigen 3 (LFA-3). *J. Exp. Med.*, **165**, 664–676.

Qin,L.H., Chavin,K.D., Lin,J.X., Yagita,H. and Bromberg,J.S. (1994) Anti-CD2 receptor and anti-CD2 ligand (CD48) antibodies synergize to prolong allograft survival. *J. Exp. Med.*, **179**, 341–346.

Sayre,P.H., Hussey,R.E., Chang,H.C., Ciardelli,T.L. and Reinherz,E.L. (1989) Structural and binding analysis of a two domain extracellular CD2 molecule. *J. Exp. Med.*, **169**, 995–1009.

Schraven,B., Samstag,Y., Altevogt,P. and Meuer,S.C. (1990) Association of CD2 and CD45 on human T lymphocytes. *Nature*, **345**, 71–74.

Seed,B. (1987) An LFA-3 cDNA encodes a phospholipid-linked membrane protein homologous to its receptor CD2. *Nature*, **329**, 840–842.

Selvaraj,P., Plunkett,M.L., Dustin,M., Sanders,M.E., Shaw,S. and Springer,T.A. (1987) The T lymphocyte glycoprotein CD2 binds the cell surface ligand LFA-3. *Nature*, **326**, 400–403.

Semnani,R.T., Nutman,T.B., Hochman,P., Shaw,S. and van Seventer,G.A. (1994) Costimulation by purified intercellular adhesion molecule 1 and lymphocyte function-associated antigen 3 induces distinct proliferation, cytokine and cell surface antigen profiles in human 'naive' and 'memory' $CD4^+$ T cells. *J. Exp. Med.*, **180**, 2125–2135.

Sido,B., Otto,G., Zimmermann,R., Müller,P., Meuer,S. and Dengler,T.J. (1996) Prolonged allograft survival by the inhibition of costimulatory CD2 signals but not by modulation of CD48 (CD2 ligand) in the rat. *Transplant. Int.*, **9**, S323–S327.

Sido,B., Otto,G., Zimmermann,R., Müller,P., Meuer,S.C. and Dengler,T.J. (1997) Modulation of the CD2 receptor and not disruption of the CD2/CD48 interaction is the principal action of CD2-mediated immunosuppression in the rat. *Cell. Immunol.*, **182**, 57–67.

Siliciano,R.F., Pratt,J.C., Schmidt,R.E., Ritz,J. and Reinherz,E.L. (1985) Activation of cytolytic T lymphocyte and natural killer cell function through the T11 sheep erythrocyte binding protein. *Nature*, **317**, 428–430.

Somoza,C., Driscoll,P.C., Cyster,J.G. and Williams,A.F. (1993) Mutational analysis of the CD2/CD58 interaction: the binding site for CD58 lies on one face of the first domain of human CD2. *J. Exp. Med.*, **178**, 549–558.

Springer,T.A., Dustin,M.L., Kishimoto,T.K. and Marlin,S.D. (1987) The lymphocyte function-associated LFA-1, CD2 and LFA-3 molecules: cell adhesion receptors of the immune system. *Annu. Rev. Immunol.*, **5**, 223–252.

Sultan,P., Schechner,J.S., McNiff,J.M., Hochman,P.S., Hughes,C.C.W., Lorber,M.I., Askenase,P.W. and Pober,J.S. (1997) Blockade of CD2–LFA-3 interactions protects human skin allografts in immunodeficient mouse/human chimeras. *Nature Biotechnol.*, **15**, 759–762.

Teunissen,M.B.M., Rongen,H.A.H. and Bos,J.D. (1994) Function of adhesion molecules lymphocyte function-associated antigen-3 and intercellular adhesion molecule-1 on human epidermal Langerhans cells in antigen-specific T cell activation. *J. Immunol.*, **152**, 3400–3409.

van der Merwe,P.A., Brown,M.H., Davis,S.J. and Barclay,A.N. (1993) Affinity and kinetic analysis of the interaction of the cell adhesion molecules rat CD2 and CD48. *EMBO J.*, **12**, 4945–4954.

van der Merwe,P.A., Barclay,A.N., Mason,D.W., Davies,E.A., Morgan,B.P., Tone,M., Krishnam,A.K.C., Ianelli,C. and Davis,S.J. (1994) Human cell-adhesion molecule CD2 binds CD58 (LFA-3) with a very low affinity and an extremely fast dissociation rate but does not bind CD48 or CD59. *Biochemistry*, **33**, 10149–10160.

Vuister,G.W. and Bax,A. (1993) Quantitative J correlation: a new approach for measuring homonuclear three-bond J (H^NH^α) coupling constants in ^{15}N enriched proteins. *J. Am. Chem. Soc.*, **115**, 7772–7777.

Wallich,R., Bernner,C., Brand,Y., Roux,M., Reister,M. and Meuer,S. (1998) Gene structure, promoter characterization and basis for alternative mRNA splicing of the human *CD58* gene. *J. Immunol.*, **160**, 2862–2871.

Wallner,B.P., Frey,A.Z., Tizard,R., Mattaliano,R.J., Hession,C., Sanders,M.E., Dustin,M.L. and Springer,T.A. (1987) Primary structure of lymphocyte function-associated antigen 3 (LFA-3). The ligand of the T lymphocyte CD2 glycoprotein. *J. Exp. Med.*, **166**, 923–932.

Walters,K.J., Dayie,K.T., Reece,R.J., Ptashne,M. and Wagner,G. (1997) Structure and mobility of the PUT3 dimer. *Nature Struct. Biol.*, **4**, 744–750.

Wingren,A.G., Parra,E., Varga,M., Kalland,T., Sjogren,H.O., Hedlund,G. and Dohlsten,M. (1995) T cell activation pathways: B7, LFA-3 and ICAM-1 shape unique T cell profiles. *Crit. Rev. Immunol.*, **15**, 235–253.

Wishart,D.S. and Sykes,B.D. (1994) The ^{13}C chemical-shift index: a simple method for the identification of protein secondary structure using ^{13}C chemical-shift data. *J. Biomol. NMR*, **4**, 171–180.

Withka,J.M., Wyss,D.F., Wagner,G., Arulanandam,A.R.N., Reinherz,E.L. and Recny,M.A. (1993) Structure of the glycosylated adhesion domain of human T lymphocyte glycoprotein CD2. *Structure*, **1**, 69–81.

Wong,Y.W., Williams,A.F., Kingsmore,S.F. and Seldin,M.F. (1990) Structure, expression and genetic linkage of the mouse BCM1 (OX45 or Blast-1) antigen. Evidence for genetic duplication giving rise to the BCM1 region on mouse chromosome 1 and the CD2/LFA3 region on mouse chromosome 3. *J. Exp. Med.*, **171**, 2115–2130.

Wyss,D.F., Choi,J.S., Li,J., Knoppers,M.H., Willis,K.J., Arulanandam,A.R.N., Smolyar,A., Reinherz,E.L. and Wagner,G. (1995) Conformation and function of the *N*-linked glycan in the adhesion domain of human CD2. *Science*, **269**, 1273–1278.

Received February 2, 1999; revised and accepted April 7, 1999